Luteolin binds Src, promotes STAT3 protein ubiquitination and exerts anti-melanoma effects in cell and mouse models

Li, Ting; Fu, Xiuqiong; Liu, Bin; Wang, Xueyu; Li, Junkui; Zhu, Peili; Niu, Xiaodi; Bai, Jingxuan ; Liu, Yuxi; Lu, Xinshan; Yu, Zhi Ling

Published in:
Biochemical Pharmacology

DOI:
10.1016/j.bcp.2022.115044

Published: 01/06/2022

Document Version:
Peer reviewed version

Luteolin binds Src, promotes STAT3 protein ubiquitination and exerts anti-melanoma effects in cell and mouse models

Ting Li [a,#], Xiuqiong Fu [a,#], Bin Liu [a,#], Xueyu Wang [a], Junkui Li [a], Peili Zhu [a], Xiaodi Niu [a], Jingxuan Bai [a], Yuxi Liu [a], Xinshan Lu [b] and Zhi-Ling Yu [a,c,*]

[a] *Center for Cancer and Inflammation Research, School of Chinese Medicine, Hong Kong Baptist University, Kowloon Tong, Hong Kong, China.*

[b] *Shaanxi Engineering Laboratory for Food Green Processing and Safety Control, College of Food Engineering and Nutritional Science, Shaanxi Normal University, Xi'an, China.*

[c] *Research and Development Centre for Natural Health Products, HKBU Institute for Research and Continuing Education, Shenzhen, China .*

[*] **Corresponding author:**

Tel: +852 34112465; Fax: +852 34112465; Email: zlyu@hkbu.edu.hk

[#] These authors contribute equally to the study.

Abstract

Signal transducer and activator of transcription 3 (STAT3) has been proposed as a target for melanoma prevention. Luteolin, a bioactive flavonoid abundant in medicinal herbs, has been reported to have anti-melanoma activity *in vitro*. However, its *in vivo* anti-melanoma effects and underlying mechanisms have not been fully elucidated. In this study, ten cell lines and two mouse models (B16F10 allograft and A375 xenograft models) were used for assessing the *in vitro* and *in vivo* anti-melanoma effects of luteolin. A STAT3 over-activated stable A375 cell line was used to determine the contribution of STAT3 signaling in luteolin's anti-melanoma effects. Results showed that luteolin dose-dependently reduced the viability of melanoma cells. Luteolin also induced apoptosis in, and suppressed migration and invasion of, A375 and B16F10 melanoma cells. Mechanistically, luteolin inhibited phosphorylation of STAT3 and Src (an upstream kinase of STAT3), accelerated ubiquitin-proteasome pathway-mediated STAT3 degradation, and downregulated the expression of STAT3-targeted genes involved in cell survival and invasion in melanoma cells. Molecular modelling and surface plasmon resonance imaging showed that luteolin stably bound to the protein kinase domain of Src. Animal studies demonstrated that prophylactic administration of luteolin restrained melanoma growth and Src/STAT3 signaling in both A375 and B16F10 melanoma-bearing mice. Moreover, luteolin's anti-melanoma effects were diminished by STAT3 over-activation in A375 cells. Our findings indicate that luteolin inhibits STAT3 signaling by suppressing STAT3 activation and promoting STAT3 protein degradation in melanoma cells, thereby exhibiting anti-melanoma effects. This study provides further

pharmacological groundwork for developing luteolin as a chemopreventive agent against melanoma.

Keywords luteolin, melanoma, STAT3 signaling, STAT3 protein degradation, chemoprevention

1. Introduction

Melanoma, a highly aggressive cancer, incurs a considerable public health burden owing to the dramatic rise in incidence worldwide [1]. The 5-year survival rate for patients with distant metastatic melanoma is merely 29.8% [2]. Currently available therapies for melanoma have many shortcomings such as low response rates and severe adverse effects [3-5]. These facts make prevention an integral component to the goal of decreasing melanoma-related mortality [6].

Various signaling pathways are involved in melanoma progression, and many molecular targets have been identified for melanoma prevention [7]. Signal transducer and activator of transcription 3 (STAT3), which is constitutively activated with high frequency in melanoma, is one of the targets that have been proposed for melanoma treatment and prevention [8,9]. Activated STAT3 regulates the transcription of miscellaneous genes related to different cellular events such as cell proliferation, apoptosis and metastasis [10]. Blockade of STAT3 activation in melanoma cells has been shown to induce cell apoptosis, cause cell cycle arrest and prevent cell invasion [11-13]. Enforced expression of a dominant-negative STAT3 variant caused melanoma growth inhibition and regression, and prevented metastasis of melanoma cells *in vivo* [13,14]. Several clinical trials have been approved for using STAT3 inhibitors to treat melanoma and other tumors; however, some trials were discontinued due to severe adverse events [15-17].

Because of their biological activity and low toxicity, naturally-occurring phytochemicals have been drawing increasing attention as promising candidates for melanoma prevention

[18,19]. Luteolin (3',4',5,7-tetrahydroxyflavone) is a bioactive flavonoid abundant in medicinal herbs, fruits and vegetables [20]. Previous studies have revealed that luteolin exerts inhibitory effects on cell growth of multiple types of cancer [20,21]. In melanoma cells, luteolin has been shown to inhibit proliferation, induce apoptosis, and reverse hypoxia-induced epithelial-mesenchymal transition (EMT) [22-25]. However, its *in vivo* anti-melanoma effects and underlying mechanisms remain to be investigated. Luteolin has been reported to inhibit STAT3 signaling in pancreatic cancer, breast cancer, cholangiocarcinoma, carcinoma and hepatoma cells [26-30]. However, whether luteolin inhibits STAT3 signaling in melanoma cells and whether STAT3 signaling inhibition contributes to luteolin's anti-melanoma effects are still unknown.

In the present study, we for the first time investigated the impact of luteolin on STAT3 signaling in melanoma cells, and established the role of STAT3 signaling inhibition in the anti-melanoma effects of luteolin. This study provides pharmacological groundwork for developing luteolin as a chemopreventive agent against melanoma.

2. Materials and methods

2.1. Materials

Luteolin (Fig. 1A) and anti-GAPDH antibody were obtained from Santa Cruz Biotechnology (Santa Cruz, CA, USA). Dimethyl sulfoxide (DMSO) was supplied by Sigma-Aldrich (St. Louis, MO, USA). The antibodies against phospho-STAT3 (Tyr705), STAT3, phospho-Src (Tyr416), Src, cleaved-PARP, PARP, Mcl-1, Bcl-xL, MMP-2, MMP-9, and K48-linked

ubiquitin were purchased from Cell Signaling Technology (Beverly, MA, USA). The primers used in this study were synthesized by Invitrogen (Casecade Biologics, CA, USA). The stock solution of luteolin (100 mM) was prepared with DMSO and stored at -20°C.

2.2. Cell culture

The human melanoma cell lines A375, A2058, COLO-829, G361, HS294T, MeWo, SK-MEL-5, SK-MEL-28 and the murine melanoma cell line B16F10 were obtained from American Type Culture Collection (Manassas, VA, USA). Human melanoma cell line IGR-1 was purchased from CLS Cell Lines Service (Eppelheim, Germany). Human keratinocyte cell line HaCaT and human adult dermal fibroblasts HDFa were obtained from Invitrogen (Casecade Biologics, Invitrogen cell culture, CA). A stable STAT3 over-activated A375 cell line (A375-STAT3C) and an empty vector-transfected stable cell line A375-EV, which were previously established by us [31], were maintained in DMEM (GIBCO, USA) supplemented with 10% FBS (GIBCO, USA) and 0.5 mg/mL G418 (Thermo Fisher, MA, USA).

2.3. Cell viability assay

The cytotoxic effects of luteolin on human melanoma cells were determined by MTT assays. Cells (5000 cells/well) seeded in 96-well microculture plates were incubated with different concentrations of luteolin for 24 h or 48 h. Afterward, 10 μL of MTT solution (5mg/ml, Thermo Fisher, MA, USA) was added to each well. The solution in each well was then removed after reacting for 2 hours. The formed formazan crystals in each well were dissolved in 100 μL of DMSO. The optical absorbance at wavelength 570 nm was detected by a microplate spectrophotometer (BD Biosciences, San Jose, CA). The cytotoxic effect of

luteolin on B16F10 cells was examined by crystal violet staining assays. Cells (2.5×10^4) were seeded in 6-well plates and incubated with various concentrations of luteolin for 24 h or 48 h. After treatment, cells were fixed with 10% formalin (Sigma-Aldrich, St. Louis, MO, USA) for 5 min and stained with 0.05% crystal violet (Sigma-Aldrich, St. Louis, MO, USA) solution in distilled water for 30 min. Cells were then washed and photographed.

2.4. Apoptosis assay

Apoptosis was determined by flow cytometry using the PE Annexin V Apoptosis Detection Kit (BD Biosciences, San Jose, CA, USA). Detached and adherent cells were collected, washed twice with cold PBS, and then resuspended in 100 μL of 1× binding buffer containing 5 μL of PE Annexin V and 5 μL of 7-AAD. After incubation in the dark at room temperature for 15 min, 400 μL of 1× binding buffer was added to each tube. Cells that were positive for PE Annexin V or 7-AAD or both were analyzed using a FACSCalibur™ cytometer (BD Biosciences, USA), with 10,000 events recorded.

2.5. In vitro cell migration and invasion assays

To test the effect of luteolin on melanoma cell migration, wound healing assays were performed. Cells grown to 80-90% confluence (6-well plate) were pre-treated with Mitomycin C (Sigma-Aldrich, St. Louis, MO, USA) to inhibit cell growth 1 h before scratching. Cell monolayers were wounded by scratching with a sterile 10 μL pipette tip across the center of the well and then treated with vehicle control or luteolin in serum-free DMEM. Cells were imaged at the 0 and 24 h time points using a microscope (Leica DMIRB).

The invasiveness of melanoma cells was analyzed using the 8-μM pore BD BioCoat™Matrigel™ invasion chamber (24 well plate). Briefly, 1.5×10^5 cells in 500 μL of DMEM-0.1% BSA supplemented with luteolin or vehicle were seeded into the upper chamber, and 750 μL of DMEM with 10% FBS was added into the lower chamber. After incubation at 37°C for 24 h, cells remaining in the upper chamber were removed with a cotton swab, and cells migrating to the lower surface of the membrane were fixed with 4% paraformaldehyde (Sigma-Aldrich, St. Louis, MO, USA) followed by staining with 0.05% crystal violet for 30 min. The invaded cells were imaged and counted from 5 randomly selected fields using a microscope (Leica DMIRB).

2.6. Western blotting

Lysates were prepared from melanoma cells and melanoma tissues. Standard Western blotting assays were performed with antibodies against phospho-STAT3 (Tyr705), STAT3, phospho-Src (Tyr416), Src, cleaved-PARP, PARP, Mcl-1, Bcl-xL, MMP-2, MMP-9, and K48-linked ubiquitin. Equal protein sample loading was monitored using an anti-GAPDH antibody. Immunoreactive bands were visualized using an ECL detection kit (Invitrogen, USA) following the manufacturer's instructions.

2.7. Real-time quantitative polymerase chain reaction (RT-qPCR)

Total RNA was extracted with Trizol reagent (Invitrogen) and reverse-transcribed into cDNA using the PrimeScript™ RT Reagent Kit (Takara, Japan) following the manufacturer's protocol. The cDNA was subjected to RT-qPCR analysis using iTaq™ Universal SYBR Green Supermix (Bio-Rad, USA) with a ViiA 7 Real Time PCR System (Applied Biosystems,

148 USA). The relative gene expression levels were calculated using the $2^{-\Delta\Delta Ct}$ method, where
149 ΔCt is the difference in cycle threshold values between the target genes and GAPDH, and
150 ΔΔCt is the difference in ΔCt values between the treatment and vehicle control. Details of
151 primer sequences for GAPDH, Mcl-1, Bcl-xL, MMP-2, MMP-9 and STAT3 are shown in
152 Table 1.

153 **2.8. Molecular modelling**

154 Molecular docking was performed using Autodock Vina (Scripps Research Institute, USA)
155 with the crystal structure of Src kinase domain in complex with Cgp77675 (PDB ID: 1YOL).
156 The Src protein for molecular docking simulation was prepared by removing the original
157 ligands and all water molecules, and adding hydrogen atoms and charges where appropriate.
158 YASARA was used for energy minimization of the ligands. The best conformation with the
159 lowest energy was selected and then subjected to molecular dynamics (MD) simulation to
160 check its stability using YASARA. All MD simulations were run with the AMBER ff99SB
161 force field. The receptor-ligand complex was put in a dodecahedron box and solvated with
162 0.9% NaCl with a distance of 5 Å between the solute and the box. Simulations were run at
163 298 K followed by simulated annealing minimizations, and velocities were scaled down by
164 0.9 every ten steps for a total time of 5 ps in 500 steps. The temperature of the system was
165 adjusted using a Berendsen thermostat based on the time-averaged temperature. After that, 50
166 ns MD simulations were performed with time steps of 2 fs and the simulation snapshots were
167 saved every 10 ps. All structure figures were generated using PyMol v.1.3, and the interaction
168 plot was generated by Ligplot+.

2.9. Surface plasmon resonance imaging (SPRi)

The binding of luteolin against Src was performed using the SPRi system (PlexArray™ HT, Plexera, USA) as previously described with some modifications [32]. Briefly, luteolin at the concentrations of 5, 10 and 20 μM were printed onto the biochip and immobilized by photo-crossing reactions. The prepared sensor chip was then inserted into the instrument and the src protein samples were prepared in Tris buffer solution (Sigma-Aldrich, St. Louis, MO, USA, 20 mM Tris, 100 mM NaCl, pH 7.5). The binding of src protein to luteolin was detected by monitoring the reflectivity variations across the sensor surface during running cycles. For each cycle, PBS (Sigma-Aldrich, St. Louis, MO, USA) running buffer was firstly flowed at a constant rate of 2 μL/s through the sensor surface to obtain a stable signal, and the protein samples were then injected at 5 μL/s for 300 s of binding, followed by 300 s of dissociation with running buffer at 2 μL/s and 200 s of regeneration with regeneration buffer (10 mM glycine-HCl buffer, pH 2.0, Sigma-Aldrich, St. Louis, MO, USA) at 2 μL/s. To gain the binding affinity, three different concentrations of Src protein (flowing phase) were flowed in turn. The binding signals-based standard refractive units (RU) were calibrated with 1% glycerol (Sigma-Aldrich, St. Louis, MO, USA, wt/vol) in running buffer with a known refractive index change (1,200 RU). All data were processed and analyzed using SPRi analysis software (Plexera SPR Data Analysis Module, Plexera).

2.10. Co-immunoprecipitation

Cultured cells were incubated on ice for 30 min with 800 μL of lysis buffer [25 mM Tris-HCl (pH 7.4), 150 mM NaCl, 1% Nonidet P-40, 1 mM EDTA and 5% glycerol] containing

protease inhibitors. The lysates were collected and centrifuged at 13,000 g for 20 min at 4°C. The supernatants were pre-cleared with 20 μL of Protein A/G PLUS Agarose (Santa Cruz Biotechnology) for 1 h at 4°C. The pre-cleared lysates were incubated with 1 μg of an anti-STAT3 antibody overnight followed by the addition of Protein A/G PLUS Agarose for 2 h. The beads were then collected and washed three times with the lysis buffer. The proteins bound to the beads were eluted by boiling with SDS sample buffer and then subjected to immunoblotting assays with an anti-ubiquitin antibody.

2.11. Animal experimentation

All animal experiments were carried out in accordance with the National Institutes of Health guide for the care and use of Laboratory animals (NIH Publications No. 8023, revised 1978). Experimental procedures were approved by and conducted following the guidelines of the Committee on the Use of Human and Animal Subjects in Teaching and Research, Hong Kong Baptist University (Approval number: HASC/16-17/0213). Male C57BL/6 mice (6-week old) and male nu/nu BALB/c mice (6-week old) were obtained from the Laboratory Animal Services Centre, the Chinese University of Hong Kong. All nu/nu BALB/c mice were maintained in individual ventilated cages in a specific animal handling room of Hong Kong Baptist University.

For the B16F10 allograft model, C57BL/6 mice were inoculated subcutaneously in the flanks with B16F10 cells (5×10^5/mice). Mice were then randomly divided into 3 groups of 7 each and intraperitoneally treated with PBS as the vehicle control or 10 mg/kg (1.1 mg/kg of human equivalent dose) or 20 mg/kg of luteolin daily for 14 consecutive days. To establish

the A375 xenograft model, male nu/nu BALB/c mice were inoculated subcutaneously in the flanks with A375 cells (5×10^6/mice). Immediately after cell injection, mice were randomly assigned to 2 groups (5 mice/group) and intraperitoneally injected with PBS as the vehicle control or 10 mg/kg of luteolin for 21 consecutive days. Body weight and tumor volume of all mice were measured at the indicated days. To monitor toxicities of luteolin, general clinical observations were made daily. These observations included, but were not limited to, changes in skin, fur, eyes, mucous membranes, occurrence of secretions and excretions and autonomic activities (e.g., lacrimation, piloerection, pupil size, unusual respiratory pattern). Changes in gait, posture and response to handling as well as the presence of colonic or tonic movements, stereotypes (e.g., excessive grooming, repetitive circling) or bizarre behaviors (e.g., self-mutilation, walking backwards) were also recorded. Food and water consumption for each group were measured once every 3 days. At the end of the experimental period, all mice were sacrificed and the tumors were collected, weighed and photographed. The organs including liver, kidneys, adrenals, testes, epididymides, spleen, brain and heart of each mouse were trimmed of any adherent tissue and weighed. Gross necropsy was performed for all the dissected organs and tissues.

2.12. Statistical analysis

All data were presented as mean ± SD. Statistical analysis was performed by ANOVA followed by Fisher's Least Significant Difference (LSD) Test using IBM SPSS Statistics Version 20.0 (IBM Corp., Armonk, New York). $P<0.05$ was regarded as statistically significant.

3. Results

3.1. Luteolin reduced cell viability and induced apoptosis in melanoma cells

Luteolin has been reported by others to possess cytotoxicity against human OCM-1, HMB-2 and A375 melanoma cells [22-24]. Here, we evaluated the cytotoxic effects of luteolin on more human melanoma cells using the MTT assay. Murine B16F10 melanoma cells can produce melanin, which may interfere with the absorbance readings in MTT assays. Therefore, the effects of luteolin on the viability of B16F10 cells were determined by crystal violet staining assays. As shown in Figs. 1B and 1C, luteolin dose- and time-dependently reduced the viabilities of both A375 and B16F10 cells. The IC_{50} values of luteolin against A375 cells were 79.61 μM and 15.43 μM for 24-h and 48-h treatments, respectively. Luteolin also exhibited dose-dependent cytotoxic effects in other melanoma cell lines including IGR-1, SK-MEL-5, COLO-829, G361, HS294T, A2058 and MEWO cells (Fig. 1D). The proliferation inhibiting rates of 30 μM of luteolin in human HDFa (32.9%, $P < 0.01$) and HaCaT (45.1%, $P < 0.01$) normal skin cells were significantly lower than in A375 cells (63.2%) (Fig. 1E).

To determine whether luteolin induced melanoma cell apoptosis, Annexin V/7-AAD double staining assays were conducted. The flow cytometry scatter plots illustrated that luteolin dose-dependently induced both early and late apoptosis in A375 cells (Fig. 1F). Statistical results showed that 20 μM and 30 μM of luteolin at 48 h remarkably increased apoptotic cell ratios to 26.5% and 43.4%, respectively, compared to control cells (8.8%) (Fig. 1G). The cleavage of poly (ADP-ribose) polymerase (PARP) is a hallmark of apoptosis. As

shown in Fig. 1H, the pro-apoptotic effect of luteolin was confirmed by the dramatic elevation of cleaved-PARP level in A375 cells after luteolin treatment.

3.2. Luteolin attenuated the migratory and invasive potential of melanoma cells

In B16F10 cells, luteolin has been demonstrated by Ruan *et al* to block hypoxia-induced EMT, the first step of the metastatic cascade [25,33]. Here, we investigated the effects of luteolin on melanoma cell migration and invasion using wound healing assays and matrigel invasion assays, respectively. As depicted in Figs. 2A and 2B, A375 and B16F10 cells tended to migrate to the wound area after culturing for 24 h, while luteolin (5 μM) treatment obviously inhibited cell migration. The results of cell invasion assay showed that luteolin (5 μM) treatment for 24 h significantly inhibited the invasion of A375 and B16F10 cells. The cell invasion rates were remarkably reduced by 37.6% (P<0.01) in luteolin-treated A375 cells and 39.0% (P<0.05) in luteolin-treated B16F10 cells, compared to that in corresponding vehicle-treated cells. In the vehicle-treated cells, the invasion rate was regarded as 100% (Figs. 2C and 2D). It was shown that 5 μM of luteolin at 24 h did not significantly affect the cell viability of either A375 or B16F10 cells. These results indicate that luteolin at the dose of 5 μM strongly inhibits melanoma cell migration and invasion.

3.3. Luteolin inhibited STAT3 signaling in melanoma cells

Having seen that luteolin inhibits melanoma cell survival, migration and invasion, we wanted to know the underlying molecular mechanisms. Previous studies have shown that luteolin inhibits STAT3 signaling and Src activation in several types of cancer other than melanoma [26-30,34]. Constitutively active STAT3 has been demonstrated to play critical roles in

melanoma development [11,12]. The non-receptor tyrosine kinase Src is an upstream kinase that can activate STAT3 [11,12]. Mcl-1 and Bcl-xL are STAT3-target genes involved in cell survival, and matrix metalloproteinase (MMP)-2 and MMP-9 are STAT3-target genes involved in cell migration and invasion [10]. Our immunoblotting results showed that luteolin (10, 20 and 30 μM) treatment for 48 h prominently decreased the protein levels of Tyr-416 phosphorylated Src, Tyr-705 phosphorylated STAT3, Mcl-1, MMP-2 and MMP-9 in both A375 and B16F10 cells (Figs. 3A and 3B). It was noteworthy that luteolin apparently lowered the protein level of total STAT3, but did not affect the protein level of total Src in A375 and B16F10 cells. RT-qPCR analyses revealed that luteolin (5, 10 and 20 μM, 24 h) markedly decreased mRNA levels of Mcl-1, MMP-2 and MMP-9 in both A375 and B16F10 cells (Fig. 3C). These findings demonstrate that luteolin suppresses STAT3 signaling in melanoma cells.

3.4. Luteolin directly bound to Src protein

To explore the detailed molecular basis underlying luteolin-mediated inhibition of STAT3 signaling, molecular modelling experiments for predicting the interaction between luteolin and Src were carried out using the docking software Autodock Vina. We found that luteolin was docked into the protein kinase domain of Src protein (PDB: 1Y0L) with a free binding energy of -8.5 kcal/mol. As shown in Figs. 4A and 4B, luteolin fitted into the hydrophobic pocket of Src protein and formed hydrogen bonds with Ser347, Met343, Thr340 and Lys279 residues. The distance of hydrogen bonds between Luteolin and Ser347, Met343, Thr340 and Lys279 were 2.88Å, 2.81Å, 2.99Å and 3.15Å, respectively (Fig. 4B). To verify the docking results, the best binding conformation of the Src-luteolin complex obtained from docking

295 analysis was then taken as the initial conformation for molecular dynamics (MD) simulation.
296 As shown in Fig. 4C, the backbone root-mean-square deviation (RMSD) profile fluctuated
297 from 1.32 Å to 3.24 Å for Src protein with no ligand and from 1.52 Å to 3.16 Å for the
298 Src-luteolin complex during the entire simulation, indicating high similarity between the two
299 structures. Besides, the Src-luteolin complex exhibited high thermodynamic stability, as
300 evidenced by the relatively higher potential energy of the Src-luteolin complex compared to
301 unbound Src (Fig. 4D). Analysis of the final pose of Src-luteolin complex after 50 ns MD
302 simulation revealed that luteolin stably penetrated into the binding site of Src (Fig. 4E).

303 Furthermore, SPRi, a powerful label-free detection system for molecular interaction
304 analysis, was conducted to validate the binding of luteolin to Src protein. As shown in Fig. 4F,
305 luteolin rapidly and concentration-dependently binds to Src protein with an equilibrium
306 dissociation constant (K_D) of 3.58×10^{-8} M. The value of K_D represents the dissociation
307 degree of the complex, and the smaller the K_D, the stronger is the binding affinity. The result
308 of SPRi indicated that luteolin showed a strong binding affinity toward Src, which verified
309 the direct binding of luteolin with Src. Taken together, our results demonstrate that luteolin
310 stably binds to the protein kinase domain of Src.

311 **3.5. Luteolin promoted ubiquitin-proteasome pathway (UPP)-mediated degradation of**
312 **STAT3 in A375 cells**

313 Considering the reduction of total STAT3 protein after luteolin treatment, we first determined
314 whether luteolin inhibits STAT3 transcription. RT-qPCR analysis showed that luteolin
315 treatment for 24 h did not affect the mRNA level of STAT3 (Fig. 4G). To evaluate whether

316 luteolin affects STAT3 stability, the protein degradation of STAT3 in A375 cells treated with
317 luteolin (30 μM) or vehicle in the presence of a protein synthesis inhibitor cycloheximide
318 (100 μg/ml) was determined. As shown in Figs. 4H and 4I, the half-life of STAT3 protein in
319 vehicle-treated A375 cells, under the selected conditions, was approximately 10 h, while
320 luteolin significantly shortened the half-life of STAT3 to about 4 h. To further obtain insight
321 into the mechanism by which luteolin promotes STAT3 degradation, A375 cells were
322 pretreated with a proteasome inhibitor MG132 or a lysosome inhibitor chloroquine (CQ) for
323 1 h, followed by luteolin or vehicle treatment for 24 h. MG132 completely reversed
324 luteolin-induced STAT3 degradation, while CQ did not block luteolin-induced STAT3
325 downregulation (Figs. 4J and 4K). Next, we determined the effect of luteolin on
326 ubiquitination of STAT3 using immunoprecipitation. To achieve this, A375 cells were
327 transiently transfected with a STAT3 expression vector (pcDNA3-STAT3), and treated with
328 luteolin for 24 h in the presence of MG132. Cell lysates were immunoprecipitated with an
329 anti-STAT3 antibody followed by immunoblotting with an anti-ubiquitin antibody. As
330 indicated in Fig. 4L, luteolin treatment apparently induced the generation of
331 polyubiquitinated STAT3 fusion protein. These results together indicate that luteolin
332 promotes UPP-mediated degradation of STAT3, rather than inhibiting STAT3 transcription.

333 **3.6. Overexpression of STAT3C diminished luteolin-caused cell viability inhibition and**
334 **apoptosis induction in A375 cells**

335 To investigate the contribution of STAT3 signaling in the anti-melanoma effects of luteolin,
336 we used two stable cell lines named A375-STAT3C and A375-EV, which were stably

transfected with a constitutively active variant of STAT3 (STAT3C) and empty vector (EV), respectively [31]. As shown in Figs. 5A and 5B, transfection of STAT3C, in contrast to transfection with EV, remarkably elevated the protein levels of total STAT3 and phospho-STAT3 in A375 cells. MTT results demonstrated that the cell viability inhibitory rates for 10, 20 and 30 μM of luteolin (48 h) significantly decreased from 23.7, 48.7 and 62.4% in A375-EV cells to 10.4, 30.9 and 45.9% in A375-STAT3C cells, respectively (Fig. 5C). The pro-apoptotic effects of luteolin in A375-STAT3C and A375-EV cells were also compared using flow cytometric analyses. The statistical results showed that the apoptotic rates induced by 20 and 30 μM of luteolin dropped dramatically from 27.7 and 39.4% in A375-EV cells to 7.4 and 22.2% in A375-STAT3C cells, respectively (Fig. 5D). These results suggest that inhibiting STAT3 signaling contributes to luteolin's anti-melanoma effects.

3.7. Luteolin inhibited melanoma growth and STAT3 signaling in B16F10 allograft and A375 xenograft models

Based on the results of cell viability assays, a murine B16F10 melanoma cell line and a human A375 melanoma cell line with excellent tumorigenicity and high malignancy were used to establish melanoma mouse models for evaluating the *in vivo* anti-melanoma effects of luteolin. For the B16F10 allograft model, the mice inoculated with B16F10 cells were treated with vehicle control or luteolin (10 mg/kg, 20 mg/kg) for 14 consecutive days. Results showed that both 10 mg/kg and 20 mg/kg of luteolin reduced the tumor size and tumor weight, with 10 mg/kg of luteolin causing a more remarkable (63.4%) reduction in tumor weight as compared to the vehicle ($P<0.01$, Figs. 6A, 6B and 6C). Accordingly, 10 mg/kg of

luteolin was tested in A375 cell-bearing nude mice. As shown in Figs. 6F, 6G and 6H, the mice receiving luteolin (10 mg/kg) exhibited significantly smaller tumor volume and lower tumor weight than the mice receiving vehicle treatment. It is noteworthy that luteolin did not affect the body weight of C57BL/6 mice (Fig. 6D) and slightly increased the body weight of nude mice (Fig. 6I). No abnormalities were noted at necropsy of all mice at the end of the experiments, and no significant differences were observed in general behavior nor in food and water consumption between groups (data not shown). Immunoblotting results showed that luteolin apparently inhibited the activation of STAT3 and Src, and that luteolin lowered the protein level of total STAT3 in both B16F10 and A375 tumors (Figs. 6E and 6J). These data indicate that 10 mg/kg of luteolin potently inhibits melanoma growth and STAT3 signaling *in vivo*.

4. Discussion

Melanoma is a highly metastatic tumor and is the leading cause of skin cancer-related death [19]. The continuing unsatisfactory status of melanoma treatment triggers an increasing interest in exploring novel agents for melanoma management. Chemoprevention, defined as the use of natural or synthetic agents to inhibit, reverse or retard carcinogenic progression, has been suggested as an unexplored strategy in melanoma management [35]. The present study demonstrated the *in vitro* and *in vivo* anti-melanoma effects of luteolin, a naturally occurring edible flavone, in human and murine melanoma cells. In addition, inhibition of STAT3 signaling was shown to contribute to the anti-melanoma effects of luteolin. Specifically,

luteolin reduced viability, induced apoptosis, and suppressed migration and invasion of melanoma cells. The cytotoxic effects of luteolin were observed in multiple melanoma cell lines including A375, B16F10, IGR-1, SK-MEL-5, COLO-829, G361, HS294T, A2058 and MEWO cells. These anti-melanoma activities of luteolin may be attributed to its effects on downregulating Mcl-1, MMP-2 and MMP-9, which are STAT3 target genes involved in cell survival or invasion. Our animal experiments demonstrated that prophylactic administration of luteolin (10 mg/kg) potently inhibited melanoma growth in both B16F10-allografted mice and A375-xenografted mice. The dosage of 10 mg/kg/d in mice is equivalent to 1.1 mg/kg/d in humans (77 mg/d for a person weighing 70 kg). Ruan *et al* [25] has previously reported that treatment with luteolin (10 or 20 mg/kg) reduced the metastatic colonization of the lungs by 50% in a B16F10 melanoma metastasis mouse model. They found that luteolin inhibited EMT in malignant melanoma cells both *in vitro* and *in vivo*, with downregulated expression of ZEB1 (an EMT inducer). Previous studies have shown that STAT3 can directly regulate ZEB1 expression and mediate EMT progression [36]. These findings, obtained both by us and others, strongly suggest that luteolin exerts anti-melanoma effects at least partially by suppressing STAT3 signaling.

A crucial part of drug development is the assessment of a drug candidate's safety and efficacy, which is predictive of clinical outcomes of the drug product in clinical trials [37]. Luteolin is commonly found in edible vegetables, such as parsley, celery, green pepper, artichoke and perilla leaf [38]. The intraperitoneal LD_{50} value of luteolin was 180 mg/kg in mice, and its oral LD_{50} is higher [39,40]. Animal experiments also indicate that luteolin at 30

mg/kg shows no toxicity in rats (i.e. for 20 consecutive days) [38,41]. In this study, no body weight reduction and no abnormalities in clinical signs and gross pathology were observed in mice treated with luteolin, suggesting the non-toxic nature of luteolin. Indeed, luteolin has been marketed as a dietary supplement under the trade name Lutimax that assists in autoimmune, metabolic, and neurodegenerative therapies. The recommended intake is 1 Lutimax pill (25 mg of luteolin) each time, 1-3 times a day. Besides, another luteolin dietary supplement (Supersmart -Luteolin) has been marketed. Clinical trials indicate no dose-limiting toxicity of luteolin when orally administered at a dose of 100 mg/day [42]. The therapeutic efficacy of a drug also depends significantly upon its bioavailability [43]. The poor bioavailability of dietary flavonoids, which limits their biological effects *in vivo*, has been a major concern for their pharmaceutical application [44]. For luteolin, the oral bioavailability has been found to be only 26 ± 6% in rats [45]. Nevertheless, luteolin showed relatively rapid absorption and slow elimination in rats after oral administration with the t_{max} (time to reach peak plasma level) of about 1.02 h and the $t_{1/2}$ (half-life of elimination) of 4.94 h, indicating the possible accumulation of luteolin in plasma after repeated dosing [46]. Furthermore, given its ability to penetrate human skin, luteolin can also be used topically for dermatological diseases in addition to oral and intraperitoneal administrations. In summary, these evidences indicate that luteolin can be regarded as an effective and safe candidate for melanoma prevention and treatment.

STAT3 has been proposed as a pathogenic factor and therapeutic/preventive target in melanoma [9,47]. In this study, we elucidated the underlying molecular mechanisms for the

anti-melanoma activities of luteolin, focusing on STAT3 signaling. We found that luteolin markedly inhibited the activation of STAT3 and Src, and decreased the protein level of total STAT3 in A375 and B16F10 cells, as well as in B16F10 allografts and A375 xenografts. Luteolin treatments also reduced the expression of STAT3 target genes (Mcl-1, MMP-2 and MMP-9) in melanoma cells. These findings, together with previous reports that luteolin blocks the STAT3 signaling pathway in pancreatic cancer, breast cancer, cholangiocarcinoma, carcinoma and hepatoma cells [26-30], suggesting that luteolin may act as a STAT3 signaling inhibitory agent. Src is one of the upstream regulators of STAT3 and Src/STAT3 signaling plays a crucial role in melanoma development and progression [9,11]. Indeed, luteolin has been shown to bind to Src and inhibit Src kinase activity [34,48]. To further validate whether luteolin could block Src/STAT3 signaling in melanoma, we investigated the interaction between luteolin and Src protein using molecular modelling and SPRi. We found that luteolin could stably bind to the kinase domain of Src protein with a strong binding affinity. The computational results together with our experimental results suggest that luteolin inhibits Src and STAT3 activation in melanoma through directly targeting an active site of Src.

Besides inhibiting STAT3 phosphorylation, luteolin treatment also reduced the protein level of STAT3 without affecting STAT3 transcription in melanoma cells. Thus, we suspect that luteolin affects STAT3 protein stability in melanoma cells. As expected, luteolin significantly shortened the half-life of STAT3 protein, indicating that luteolin accelerated STAT3 degradation in melanoma cells. In hepatoma cells, luteolin has been shown to promote ubiquitin-dependent degradation of Tyr705-phosphorylated STAT3 [30]. In all tissues, the

majority of intracellular proteins are degraded *via* UPP, and extracellular proteins and some cell surface proteins are degraded within lysosomes [49]. Our results revealed that a proteasome inhibitor MG132 rather than a lysosome inhibitor CQ reversed luteolin-induced STAT3 degradation. Luteolin treatment also increased ubiquitin-STAT3 complexes in melanoma cells. Thus, we conclude that luteolin promotes UPP-mediated degradation of STAT3 in melanoma cells. It is well known that many target proteins for proteasomal degradation are recognized by the target-specific E3 ligase [30]. However, studies in this field are very limited. Calcineurin, TMF/ARA160 and the ubiquitin E3 ligase TRAF6 have been demonstrated to be involved in UPP-mediated STAT3 degradation [50-52]. In the future, we will determine whether these molecules are involved in luteolin-induced proteasomal degradation of STAT3 in melanoma cells.

To verify the contribution of STAT3 signaling to the anti-melanoma effects of luteolin, we determined whether STAT3 over-activation in A375 cells could counteract the anti-melanoma effects of luteolin. Results showed that STAT3C overexpression prominently diminished the viability inhibitory and pro-apoptotic effects of luteolin in A375 cells. These results demonstrated that inhibition of STAT3 signaling is one of the mechanisms underlying the anti-melanoma effects of luteolin. In this study, we found that luteolin affects STAT3 signaling in two ways. Luteolin not only blocks Src phosphorylation and suppresses STAT3 activation, but also promotes STAT3 protein degradation. Most proteins, notably transcription factors, are composed of multiple domains associated with specific functions, but traditional small-molecule antagonists mainly disrupt the activity of only one domain in the target

463 protein [53,54]. This fact is precisely one of the reasons why acquired drug resistance to
464 conventional targeted therapies occurs. In light of the above facts, targeted protein
465 degradation, which can directly abolish the presence of an oncoprotein, is believed to possess
466 certain advantages (such as increased potency and prolonged efficacy) over inhibition of its
467 activity [54]. Hence, we reasonably believe that luteolin may elicit a more pronounced and
468 longer lasting anti-melanoma consequence than common STAT3 inhibitors. In the future, we
469 will investigate whether the anti-melanoma efficacy of luteolin is better than that of STAT3
470 inhibitors.

471 In summary, our study demonstrates that luteolin exerts anti-melanoma effects *in vitro* and
472 *in vivo* without overt toxicities to normal cells and melanoma-bearing mice, and that
473 suppression of STAT3 signaling through binding to Src protein and accelerating STAT3
474 protein degradation contributes to the anti-melanoma mechanisms of luteolin (Fig. 7).
475 Previous studies have shown that luteolin has beneficial effects on skin cancers including
476 melanoma, and has relatively good bioavailability and safety [39-42,45,46,55]. Our and peers'
477 research findings indicate that luteolin has the potential to be developed into an effective and
478 safe chemopreventative agent against melanoma. Based on our experimental data, we
479 recommend clinical trials of luteolin at a non-toxic dose (10 mg/kg) for melanoma prevention
480 and treatment.

481

482 **Author contributions**

483 TL, XQF and BL performed the study, analyzed and interpreted the data, and drafted the
484 manuscript. XYW helped in the animal study and revised the manuscript. JKL, PLZ, XDN,

JXB, YXL and XSL helped in data analysis and reviewed the manuscript. ZLY designed the study, reviewed the original data, and finalized the manuscript. All authors reviewed and approved the final version of manuscript.

Conflict of interest statement

The authors declare no competing interests.

Acknowledgements

This study was supported by National Natural Science Foundation of China (81874358, 81874358, 81803788 and 82174029), Shenzhen Science and Technology Innovation Commission (JCYJ20200109150719846) and Department of Science and Technology of Guangdong Province (2021A1515010658).

References

[1] Tucker MA, Elder DE, Curry M, Fraser MC, Pichler V, Zametkin D, et al. Risks of melanoma and other cancers in melanoma-prone families over 4 decades. J Invest Dermatol 2018; 138(7): 1620-1626.

[2] Surveillance, epidemiology, and end results program. Cancer Stat Facts: melanoma of the skin. 2020. Retrieved from https://seer.cancer.gov/statfacts/html/melan.html

[3] Pasquali S, Hadjinicolaou AV, Sileni VC, Rossi CR, Mocellin S, Cochrane Skin Group. Systemic treatments for metastatic cutaneous melanoma. Cochrane Database Syst Rev 2018; 2018(2): CD011123.

[4] Bensimon AG, Zhou ZY, Jenkins M, Song Y, Gao W, Signorovitch J, et al. An economic evaluation of Pembrolizumab versus other adjuvant treatment strategies for resected high-risk stage III melanoma in the USA. Clin Drug Invest 2020; 40(7): 629-643.

[5] Diao K, Bian SX, Routman DM, Yu C, Ye JC, Wagle NA, et al. Stereotactic radiosurgery and ipilimumab for patients with melanoma brain metastases: clinical outcomes and toxicity. J Neurooncol 2018; 139(2): 421-429.

[6] Jeter J, Bowles T, Curiel-Lewandrowski C, Swetter SM, Filipp FV, Abdel-Malek Z, et al. Chemoprevention agents for melanoma: a path forward into phase III clinical trials. Cancer 2019; 125(15): 2706.
[7] Palmieri G, Ombra M, Colombino M, Casula M, Sini M, Manca A, et al. Multiple molecular pathways in melanomagenesis: characterization of therapeutic targets. Front Oncol 2015;5:183.
[8] Alcolea V, Karelia DN, PandeyMK, Plano D, Singh P, Palop JA, et al. Identification of a novel quinoxaline-isoselenourea targeting the STAT3 pathway as a potential melanoma therapeutic. Int J Mol Sci 2019; 20(3): 521.
[9] Lesinski GB. The potential for targeting the STAT3 pathway as a novel therapy for melanoma. Future Oncol 2013;9(7):925-7.
[10] Johnson DE, O'Keefe RA, Grandis JR. Targeting the IL-6/JAK/STAT3 signalling axis in cancer. Nat Rev Clin Oncol 2018; 15(4): 234-48.
[11] Niu G, Bowman T, Huang M, Shivers S, Reintgen D, Daud A, et al. Roles of activated Src and Stat3 signaling in melanoma tumor cell growth. Oncogene 2002;21(46):7001-10.
[12] Xie TX, Wei D, Liu M, Gao AC, Ali-Osman F, Sawaya R, et al. Stat3 activation regulates the expression of matrix metalloproteinase-2 and tumor invasion and metastasis. Oncogene 2004;23(20):3550-60.
[13] Fu XQ, Liu B, Wang YP, Li JK, Zhu PL, Li T, et al. Activation of STAT3 is a key event in TLR4 signaling-mediated melanoma progression. Cell Death Dis 2020; 11(4): 246.
[14] Niu G, Shain KH, Huang M, Ravi R, Bedi A, Dalton WS, et al. Overexpression of a dominant-negative signal transducer and activator of transcription 3 variant in tumor cells leads to production of soluble factors that induce apoptosis and cell cycle arrest. Cancer Res 2001;61(8):3276-80.
[15] Ogura M, Uchida T, Terui Y, Hayakawa F, Kobayashi Y, Taniwaki M, et al. Phase I study of OPB-51602, an oral inhibitor of signal transducer and activator of transcription 3, in patients with relapsed/refractory hematological malignancies. Cancer Sci 2015;106(7):896-901.
[16] Okusaka T, Ueno H, Ikeda M, Mitsunaga S, Ozaka M, Ishii H, et al. Phase 1 and pharmacological trial of OPB-31121, a signal transducer and activator of transcription-3 inhibitor, in patients with advanced hepatocellular carcinoma. Hepatol Res 2015;45(13):1283-91.
[17] Chiba T. STAT3 inhibitors for cancer therapy-the rationale and remained problems. EC Cancer 2016;1(S1):S1-S8.
[18] Chhabra G, Ndiaye MA, Garcia-Peterson LM, Ahmad N. Melanoma chemoprevention: current status and future prospects. Photochem Photobiol 2017; 93(4): 975-989.
[19] Tong LX, Young LC. Nutrition: the future of melanoma prevention? J Am Acad Dermatol 2014;71(1):151-60.
[20] Lida K, Naiki T, Naiki-Ito A, Suzuki S, Kato H, Nozaki S, et al. Luteolin suppresses bladder cancer growth via regulation of mechanistic target of rapamycin pathway. Cancer Sci 2020; 111(4): 1165-1179.

554 [21] Yu Q, Zhang M, Ying Q, Xie X, Yue S, Tong B, et al. Decrease of AIM2 mediated by
555 luteolin contributes to non-small cell lung cancer treatment. Cell Death Dis 2019; 10(3):
556 218.
557 [22] George VC, Kumar DRN, Suresh PK, Kumar S, Kumar RA. Comparative studies to
558 evaluate relative in vitro potency of luteolin in inducing cell cycle arrest and apoptosis in
559 HaCaT and A375 cells. Asian Pacific J Cancer Prev 2013;14(2):631-7.
560 [23] Kim JK, Kang KA, Ryu YS, Piao MJ, Han X, Oh MC, et al. Induction of endoplasmic
561 reticulum stress via reactive oxygen species mediated by luteolin in melanoma cells.
562 Anticancer Res 2016;36(5):2281-9.
563 [24] Li C, Wang Q, Shen S, Wei X, Li G. HIF-1α/VEGF signaling-mediated
564 epithelial-mesenchymal transition and angiogenesis is critically involved in
565 anti-metastasis effect of luteolin in melanoma cells. Phytother Res 2019; 33(3): 798-807.
566 [25] Ruan JS, Liu YP, Zhang L, Yan LG, Fan FT, Shen CS, et al. Luteolin reduces the
567 invasive potential of malignant melanoma cells by targeting β3 integrin and the
568 epithelial-mesenchymal transition. Acta Pharmacol Sin 2012;33(10):1325-31.
569 [26] Huang X, Dai S, Dai J, Xiao Y, Bai Y, Chen B, et al. Luteolin decreases invasiveness,
570 deactivates STAT3 signaling, and reverses interleukin-6 induced epithelial-mesenchymal
571 transition and matrix metalloproteinase secretion of pancreatic cancer cells. Onco Targets
572 Ther 2015;8:2989-3001.
573 [27] Yang MY, Wang CJ, Chen NF, Ho WH, Lu FJ, Tseng TH. Luteolin enhances
574 paclitaxel-induced apoptosis in human breast cancer MDA-MB-231 cells by blocking
575 STAT3. Chem Biol Interact 2014;213:60-8.
576 [28] Aneknan P, Kukongviriyapan V, Prawan A, Kongpetch S, Sripa B, Senggunprai L.
577 Luteolin arrests cell cycling, induces apoptosis and inhibits the JAK/STAT3 pathway in
578 human cholangiocarcinoma cells. Asian Pac J Cancer Prev 2014;15(12):5071-6.
579 [29] Fu J, Chen D, Zhao B, Zhao Z, Zhou J, Xu Y, et al. Luteolin induces carcinoma cell
580 apoptosis through binding Hsp90 to suppress constitutive activation of STAT3. PLoS One
581 2012;7(11):e49194.
582 [30] Selvendiran K, Koga H, Ueno T, Yoshida T, Maeyama M, Torimura T, et al. Luteolin
583 promotes degradation in signal transducer and activator of transcription 3 in human
584 hepatoma cells: an implication for the antitumor potential of flavonoids. Cancer Res
585 2006;66(9):4826-34.
586 [31] Cao HH, Tse AK, Kwan HY, Yu H, Cheng CY, Su T, et al. Quercetin exerts
587 anti-melanoma activities and inhibits STAT3 signaling. Biochem Pharmacol
588 2014;87(3):424-34.
589 [32] Deng B, Jiang XL, Tan ZB, Cai M, Deng SH, Ding WJ, et al. Dauricine inhibits
590 proliferation and promotes death of melanoma cells via inhibition of Src/STAT3 signaling.
591 Phytother Res 2021;35(7):3836-3847.
592 [33] Yang J, Antin P, Berx G, Blanpain C, Brabletz T, Bronner M, et al. Guidelines and
593 definitions for research on epithelial-mesenchymal transition. Nat Rev Mol Cell Biol
594 2020; 21(6): 341-352.

[34] Byun S, Lee KW, Jung SK, Lee EJ, Hwang MK, Lim SH, et al. Luteolin inhibits protein kinase Cε and c-Src activities and UVB-induced skin cancer. Cancer Res 2010; 70: 2415-23.
[35] Demierre MF, Nathanson L. Chemoprevention of melanoma: an unexplored strategy. J Clin Oncol 2003;21(1):158-65.
[36] Jin W. Role of JAK/STAT3 signaling in the regulation of metastasis, the transition of cancer stem cells, and chemoresistance of cancer by epithelial-mesenchymal transition. Cells 2020; 9(1): 217.
[37] Muller PY, Milton MN. The determination and interpretation of the therapeutic index in drug development. Nat Rev Drug Discov 2012;11(10):751-61.
[38] Yasuda MT, Fujita K, Hosoya T, Imai S, Shimoi K. Absorption and metabolism of luteolin and its glycosides from the extract of Chrysanthemum morifolium flowers in rats and Caco-2 Cells. J Agric Food Chem 2015;63(65):7693-9.
[39] Oswald E, Sesarman A, Franzke CW, Wölfle U, Bruckner-Tuderman L, Jakob T, et al. The flavonoid luteolin inhibits Fcγ-dependent respiratory burst in granulocytes, but not skin blistering in a new model of pemphigoid in adult mice. PLoS One 2012;7(2):e31066.
[40] Chen C, Peng W, Tsai K, Hsu S. Luteolin suppresses inflammation-associated gene expression by blocking NF-kappaB and AP-1 activation pathway in mouse alveolar macrophages. Life Sci 2007; 81:1602-14.
[41] Samy RP, Gopalakrishnakone P, Ignacimuthu S. Anti-tumor promoting potential of luteolin against 7,12-dimethylbenz(a)anthracene-induced mammary tumors in rats. Chem Biol Interact 2006; 164:1-14.
[42] Ali F, Siddique YH. Bioavailability and pharmaco-therapeutic potential of luteolin in overcoming alzheimer's disease. CNS Neurol Disord Drug Targets 2019; 18:352-365.
[43] Khan AD, Singh L. Various techniques of bioavailability enhancement: a review. J Drug Deliv Ther 2016;6(3):34-41.
[44] Gao S, Hu M. Bioavailability challenges associated with development of anti-cancer phenolics. Mini-Rev Med Chem 2010;10(6):550-67.
[45] Lin LC, Pai YF, Tsai TH. Isolation of luteolin and luteolin-7-O-glucoside from Dendranthema morifolium Ramat Tzvel and their pharmacokinetics in rats. J Agric Food Chem 2015;63(65):7700-6.
[46] Zhou P, Li LP, Luo SQ, Jiang HD, Zeng S. Intestinal absorption of luteolin from peanut hull extract is more efficient than that from individual pure luteolin. J Agric Food Chem 2008;56(1):296-300.
[47] Emeagi PU, Maenhout S, Dang N, Heirman C, Thielemans K, Breckpot K. Downregulation of Stat3 in melanoma: reprogramming the immune microenvironment as an anticancer therapeutic strategy. Gene Ther 2013;20(11):1085-92.
[48] Lee JO, Jeong D, Kim MY, Cho JY. ATP-binding pocket-targeted suppression of Src and Syk by luteolin contributes to its anti-inflammatory action. Mediators Inflamm 2015, 2015:1-12.

[49] Zhang L, Wei PF, Song YH, Dong L, Wu YD, Hao ZY, et al. $MnFe_2O_4$ nanoparticles accelerate the clearance of mutant huntingtin selectively through ubiquitin-proteasome system. Biomaterials 2019;216:119248.
[50] Yang Y, Song S, Min H, Chen X, Gao Q. STAT3 degradation mediated by calcineurin involved in the neurotoxicity of isoflurane. Neuroreport 2016;27(2):124-30.
[51] Perry E, Tsruya R, Levitsky P, Pomp O, Taller M, Weisberg S, et al. TMF/ARA160 is a BC-boxcontaining protein that mediates the degradation of Stat3. Oncogene 2004;23(55):8908-19.
[52] Ruan HH, Zhang Z, Wang SY, Nickels LM, Tian L, Qiao JJ, et al. Tumor necrosis factor receptor-associated factor 6 (TRAF6) mediates ubiquitination-dependent STAT3 activation upon Salmonella enterica Serovar Typhimurium infection. Infect Immun 2017;85(8):e00081-17.
[53] Brodsky S, Jana T, Mittelman K, Chapal M, Kumar DK, Carmi M, et al. Intrinsically disordered regions direct transcription factor in vivo binding specificity. Molecular Cell 2020; 79(3): 459-471.e4
[54] Winter GE, Buckley DL, Paulk J, Roberts JM, Souza A, Dhe-Paganon S, et al. Phthalimide conjugation as a strategy for in vivo target protein degradation. Science 2015;348(6241):1376-81.
[55] Juszczak AM, Woelfle U, Koncic MZ, Tomczyk M. Skin cancer, including related pathways and therapy and the role of luteolin derivatives as potential therapeutics. Med Res Rev 2022, online. DOI: 10.1002/med.21880.

Figure legends

Figure 1. Cytotoxic effects of luteolin in melanoma cells. (A) The chemical structure of luteolin. (B) Inhibitory effects of luteolin on the viability of A375 cells. (C) Inhibitory effects of luteolin on B16F10 cell proliferation. A375 and B16F10 cells were treated with the indicated concentrations of luteolin for 24 or 48 h, followed by the MTT assay and crystal violet staining assay. (D) Inhibitory effects of luteolin on the viabilities of A375, IGR-1, SK-MEL-5, COLO-829, G361, HS294T, A2058, MeWo and SK-MEL-28 melanoma cells. (E) Comparison of inhibitory effects of luteolin on the viability of A375 cells and normal skin cells. MTT assays were performed after cells treated with the indicated concentrations of luteolin for 48 h. For apoptosis assays, cells treated with the indicated concentrations of luteolin (48 h) were subjected to the Annexin V/7-AAD double staining assays and immunoblotting assays. (F) Representative flow cytometric dot plots. (G) The mean percentage of apoptotic cells (Q2+Q3) from three independent experiments. $^{**}P < 0.01$ versus control. (H) Effect of luteolin on PARP cleavage in A375 cells. Data are mean ± SD of three independent experiments.

Figure 2. Luteolin inhibited migration and invasion of melanoma cells. Representative photographs of A375 (A) and B16F10 (B) cell migration in the wound healing assay. Cells were treated with luteolin (5 μM) or vehicle control for 24 h. The defined areas were photographed at 0 and 24 h post-wounding. Representative photographs of invaded cells (left) and quantification of invasiveness (right) for A375 (C) and B16F10 (D) cells are shown.

Cells (1.5×10^5) in DMEM-0.1% BSA with luteolin (5 μM) or vehicle control were placed in the upper chamber and allowed to pass through a matrigel-coated membrane for 24 h. In the lower chamber, DMEM with 10% FBS served as a source of chemo-attractants. Cells that had invaded the membrane were photographed. For each replicate experiment, the average cell number in 5 randomly selected fields were measured. Data are shown as mean ± SD of three independent experiments, $^{**}P < 0.01$.

Figure 3. Luteolin suppressed STAT3 signaling in melanoma cells. Effects of luteolin on the protein levels of phospho-Src (p-Src), total Src, phospho-STAT3 (p-STAT3), total STAT3, Mcl-1 and Bcl-xL, MMP-2 and MMP-9 in A375 (A) and B16F10 (B) cells. Cells were treated with luteolin (10, 20 and 30 μM) for 48 h, and protein levels were detected by immunoblotting. GAPDH was used as a loading control. Relative expression levels of the above proteins in A375 and B16F10 cells were quantified using Image J software. (C) Luteolin decreased the mRNA levels of STAT3 target genes in melanoma cells. A375 and B16F10 cells were treated with indicated concentrations of luteolin for 24 h. The mRNA levels of Bcl-xL, Mcl-1, MMP-2 and MMP-9 were measured with RT-qPCR analysis. Results shown are fold change ± SD of three independent experiments, $^{*}P < 0.05$, $^{**}P < 0.01$ versus vehicle control.

Figure 4. Luteolin directly bound to Src protein and promoted UPP-mediated STAT3 degradation. (A-E) Molecular docking of luteolin (CID: 5280445) and Src (PDB ID: 1YOL)

699 was performed using Autodock Vina (Scripps Research Institute, USA). YASARA was used
700 for energy minimization of the ligands. The best conformation with the lowest energy was
701 selected and then subjected to MD simulation to check its stability using YASARA. (A)
702 Three-dimensional binding mode of luteolin (green) in complex with Src. The hydrogen
703 bonds were indicated with light blue lines. (B) Two-dimensional diagram demonstrating the
704 H-bonds and interactions between luteolin and Src residues Ser347, Met343, Thr340 and
705 Lys279. (C) Backbone RMSD and (D) potential energy of Src protein with no ligand
706 (Src-Unbound in red line) and in complex with luteolin (Src-Luteolin in blue line) in a 50 ns
707 MD simulation trajectory analysis. (E) Surface crystal structures of Src-luteolin complex at 0
708 ns and 50 ns. (F) The SPRi fitting curves for different concentrations of luteolin (5, 10 and 20
709 μM) toward Src. The SPRi signals are expressed as resonance units (RU). (G-K) Luteolin
710 induced ubiquitin-proteasome pathway (UPP)-mediated degradation of STAT3 in A375 cells.
711 (G) STAT3 mRNA expression in A375 cells treated with indicated concentrations of luteolin
712 for 24 h was analyzed by RT-qPCR. (H) Time course study for the protein levels of STAT3.
713 Cells were exposed to 30 μM of luteolin or vehicle in the presence of protein synthesis
714 inhibitor cycloheximide (100 μg/ml) for the indicated time periods, followed by Western blot
715 analyses. (I) The band intensity for STAT3 in (H) was quantified with Image J software. (J)
716 Cells were pretreated with MG132 (5 μM) or chloroquine (CQ, 25 μM) for 1 h, followed by
717 luteolin (30 μM) or vehicle treatment for 24 h. Protein levels were detected by
718 immunoblotting. (K) The band intensity for STAT3 in (J) was quantified with Image J
719 software. In (G), (I) and (K), data are mean ± SD of three independent experiments. $^{**}P <$

0.01 versus vehicle control. (L) Immunoprecipitation analyses of ubiquitinated STAT3 levels. A375 cells were transiently transfected with STAT3 expression vector (pcDNA3-STAT3) followed by luteolin (30 μM) or vehicle treatment for 24 h in the presence of MG132 (5 μM). Cell lysates were immunoprecipitated with anti-STAT3 antibody and immunoblotted with anti-ubiquitin and anti-STAT3 antibodies. 5% of input cell lysates were immunoblotted with anti-STAT3 and anti-GAPDH antibodies.

Figure 5. STAT3 over-activation diminished luteolin's anti-melanoma effects. (A) Expression levels of p-STAT3, STAT3 and Flag in A375-STAT3C and A375-EV stable cells. A375-STAT3C and A375-EV cells were A375 cells stably transfected with Stat3-C Flag pRc/CMV plasmid and the empty vector, respectively. Protein levels were determined by immunoblotting. GAPDH was a loading control. Results shown are the representatives of three independent experiments. (B) The band intensity in (A) was quantified with Image J software. (C) STAT3C overexpression diminished the cytotoxic effects of luteolin. (D) STAT3C overexpression diminished the pro-apoptotic effects of luteolin. In (C) and (D), A375-STAT3C and A375-EV cells were treated with luteolin (10, 20 and 30 μM) for 48 h. Cell viability was determined with MTT assays. Apoptosis was detected with Annexin V/7-AAD double staining assays. Data shown are mean ± SD of three independent experiments, $^{**}P < 0.01$, luteolin's effects in A375-STAT3C cells versus in A375-EV cells.

Figure 6. Anti-melanoma effects of luteolin in C57BL/6 mice bearing syngeneic B16F10 melanoma tumors and in nude mice bearing human A375 xenograft tumors. B16F10 cells (5 $\times 10^5$) were subcutaneously inoculated at the right flank of C57/BL6 mice. Immediately after cell injection, mice were randomly divided into three groups (n=7) and intraperitoneally administered with PBS (vehicle control), 10 or 20 mg/kg of luteolin once daily. Tumor volume and body weight of each mouse were monitored at the indicated days. At day 14, mice were sacrificed and tumors were dissected. The photos of collected B16F10 tumors (A), mean tumor weights (B), the growth curves of B16F10 tumors (C), and body weight curves (D) are shown. (E) Protein levels of p-STAT3 (Tyr705), STAT3, p-Src (Tyr416) and Src in B16F10 tumors tissues from 2 individual mice in each group were determined by immunoblotting (left), and the relative band intensity was analyzed by Image J (right). For A375 xenograft model, nude mice (n=5) were intraperitoneally administered with PBS (vehicle control) or luteolin (10 mg/kg) once daily immediately after subcutaneous inoculation of A375 cells (5 $\times 10^6$) at the right flank of each mouse. The photos of collected A375 xenografts (F), mean tumor weights (G), the growth curves of A375 xenografts (H) and body weight curves (I) are shown. The word 'None' on (F) means no tumor was found on the back of the mouse. (J) Protein levels of p-STAT3 (Tyr705), STAT3, p-Src (Tyr416) and Src in A375 xenografts from 3 individual mice in each group were examined by immunoblotting (left), and the relative band intensity was quantified using Image J (right). Data shown are mean ± SD. $^*P < 0.05$, $^{**}P < 0.01$ versus vehicle control group.

761 **Figure 7.** A schematic summary for the anti-melanoma mechanisms of luteolin (Lu).
762 Suppression of STAT3 signaling through inhibiting Src activation and accelerating STAT3
763 protein degradation contributes to the anti-melanoma mechanisms of luteolin.
764

765 **Table 1. Gene-specific primer sequences employed in RT-qPCR.**

Gene	Forward primer (5’-3’)	Reverse primer (5’-3’)
STAT3 (human)	GAGAAGGACATCAGCGGTAAG	CAGTGGAGACACCAGGATATTG
GAPDH (human)	CTGCACCACCAACTGCTTAGC	CTTCACCACCTTCTTGATGTC
MMP-2 (human)	AAGTGGTCCGTGTGAAGTATG	GGTATCAGTGCAGCTGTTGTA
MMP-9 (human)	GAACTTTGACAGCGACAAGAAG	CGGCACTGAGGAATGATCTAA
Mcl-1 (human)	AAGCCAATGGGCAGGTCT	TGTCCAGTTTCCGAAGCAT
Bcl-xl (human)	ATGAACTCTTCCGGGATGG	TGCAATCCGACTCACCAATA
GAPDH (mouse)	CCATGGAGAAGGCCGGGG	CAAAGTTGTCATGGATGACC
MMP-2 (mouse)	CTGGAATGCCATCCCTGATAA	GGTTCTCCAGCTTCAGGTAATAA
MMP-9 (mouse)	CTGGAACTCACACGACATCTT	TCCACCTTGTTCACCTCATTT
Mcl-1 (mouse)	TGTAAGGACGAAACGGGACT	AAAGCCAGCAGCACATTTCT
Bcl-xl (mouse)	TTCGGGATGGAGTAAACTGG	TGTCCAGTTTCCGAAGCAT

766

767 **Figure 1**

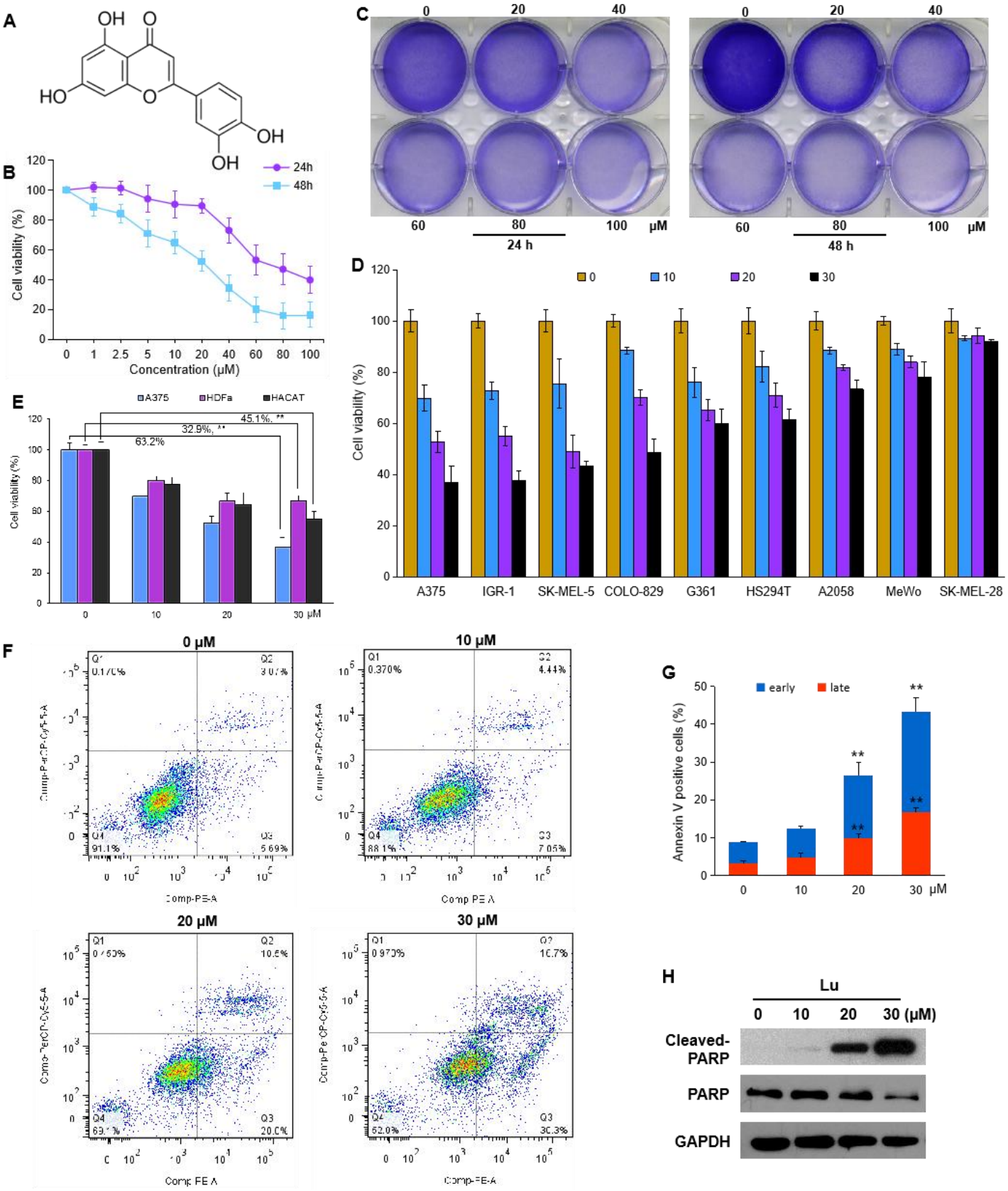

768

769

Figure 2

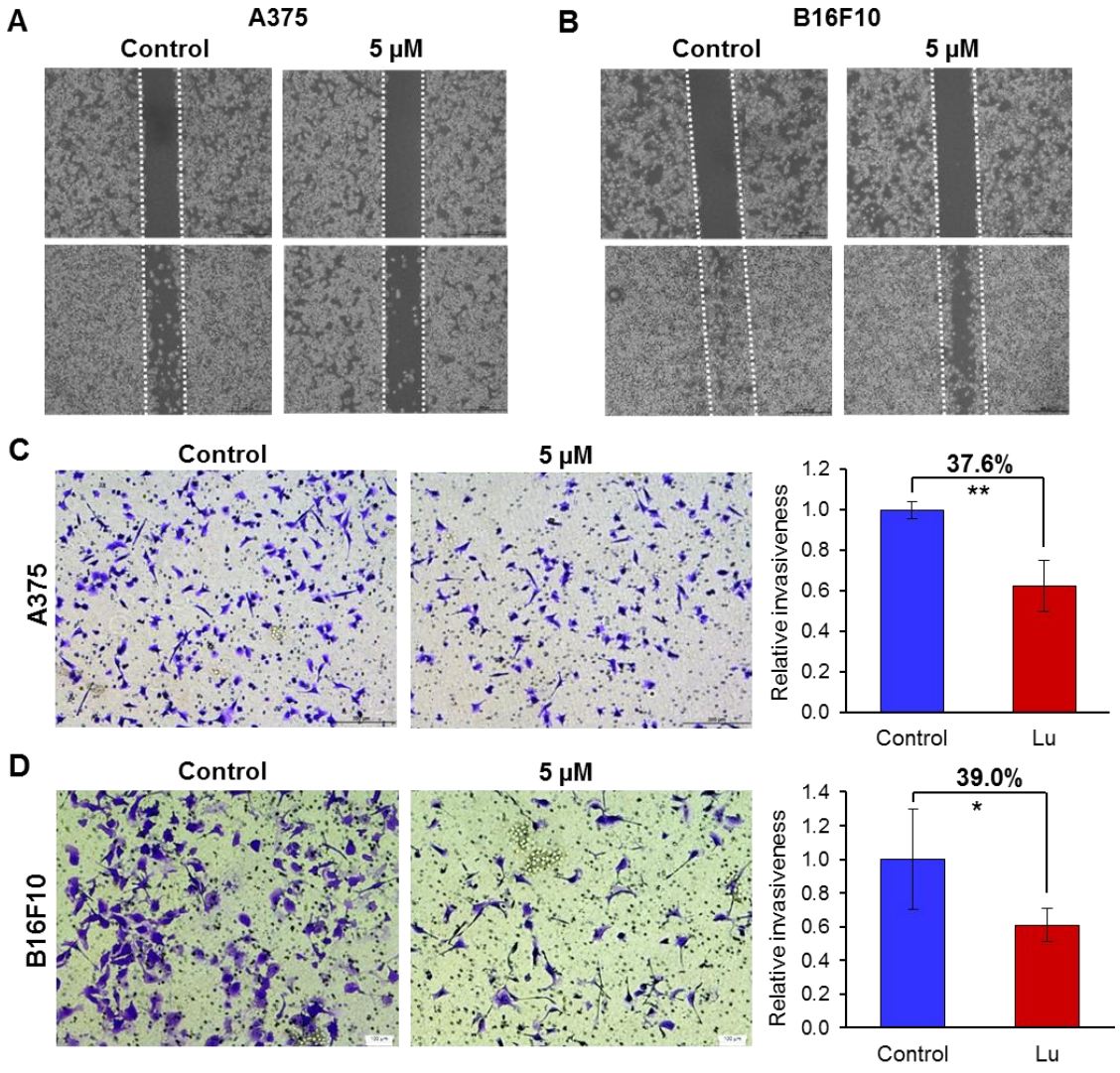
A
A375
Control
5 μM
B
B16F10
Control
5 μM
C
Control
5 μM
A375
Relative invasiveness
37.6%
**
Control
Lu
D
Control
5 μM
B16F10
Relative invasiveness
39.0%
*
Control
Lu

773 **Figure 3**

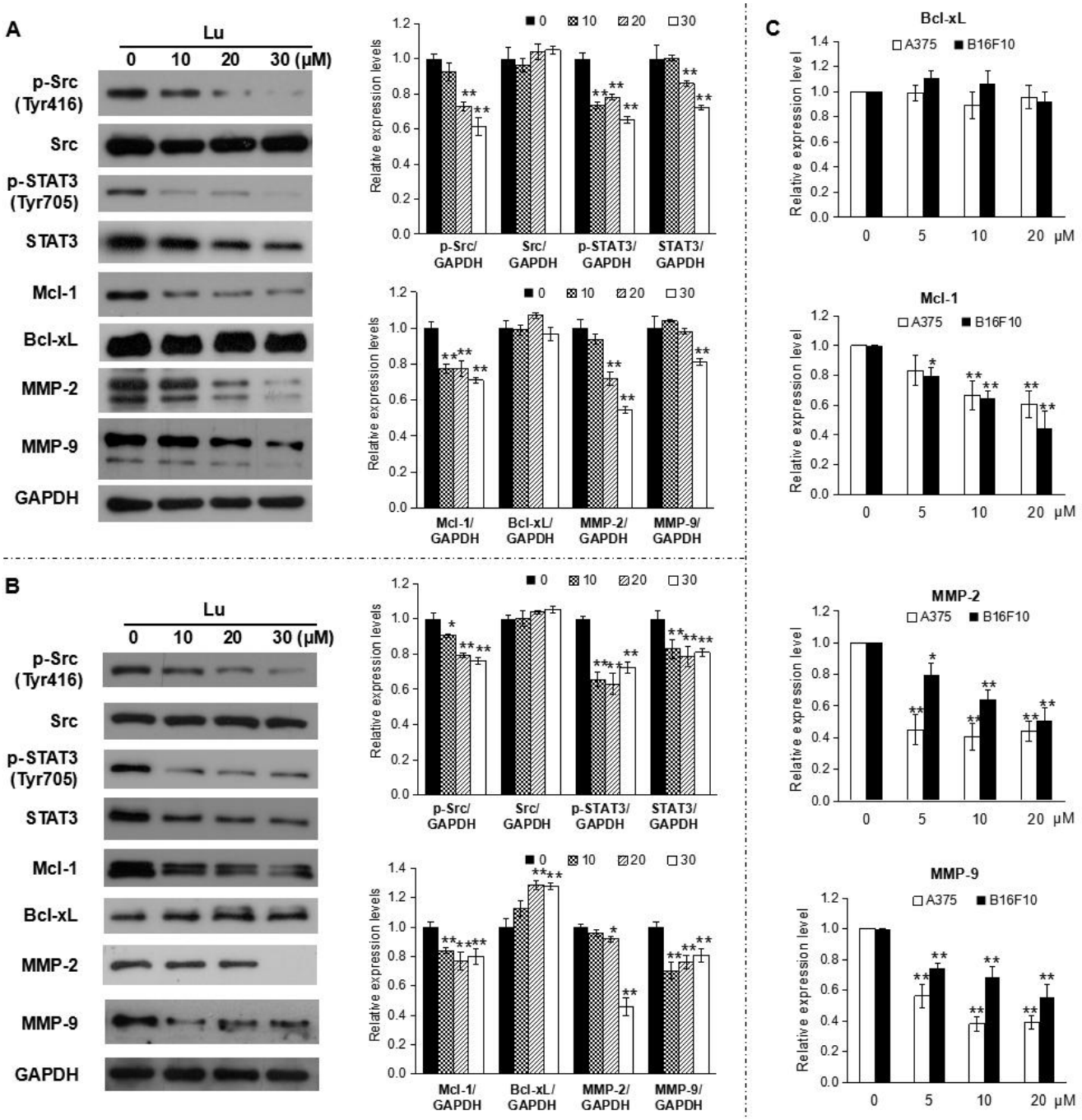

774

775

776 **Figure 4**

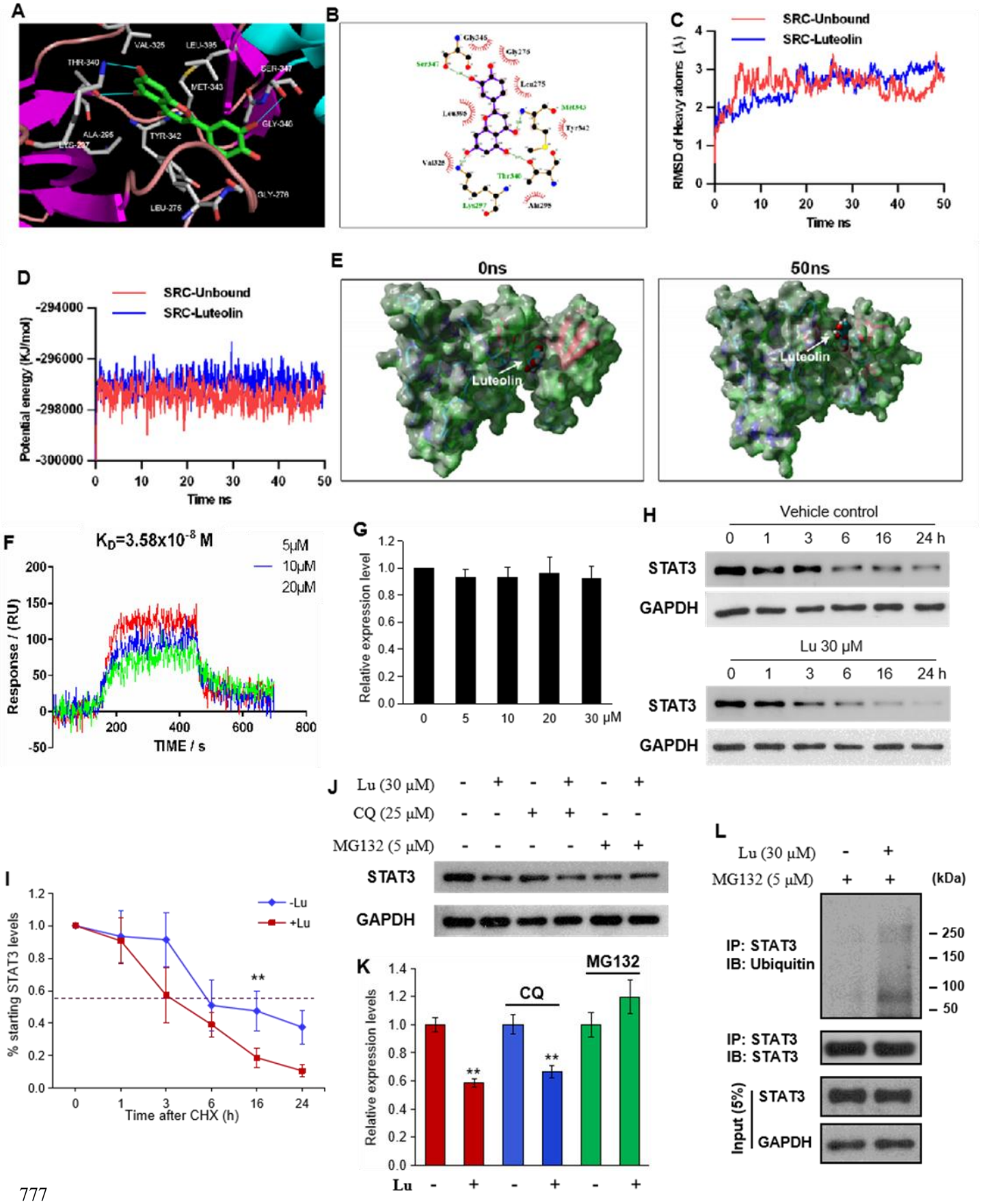

777

778 **Figure 5**

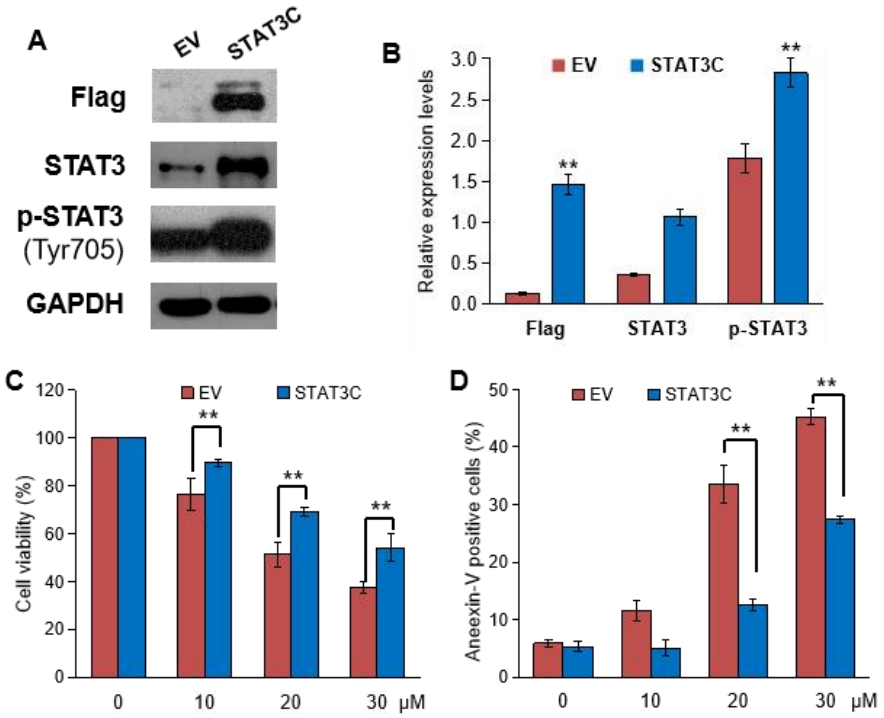

779

780

781 **Figure 6**

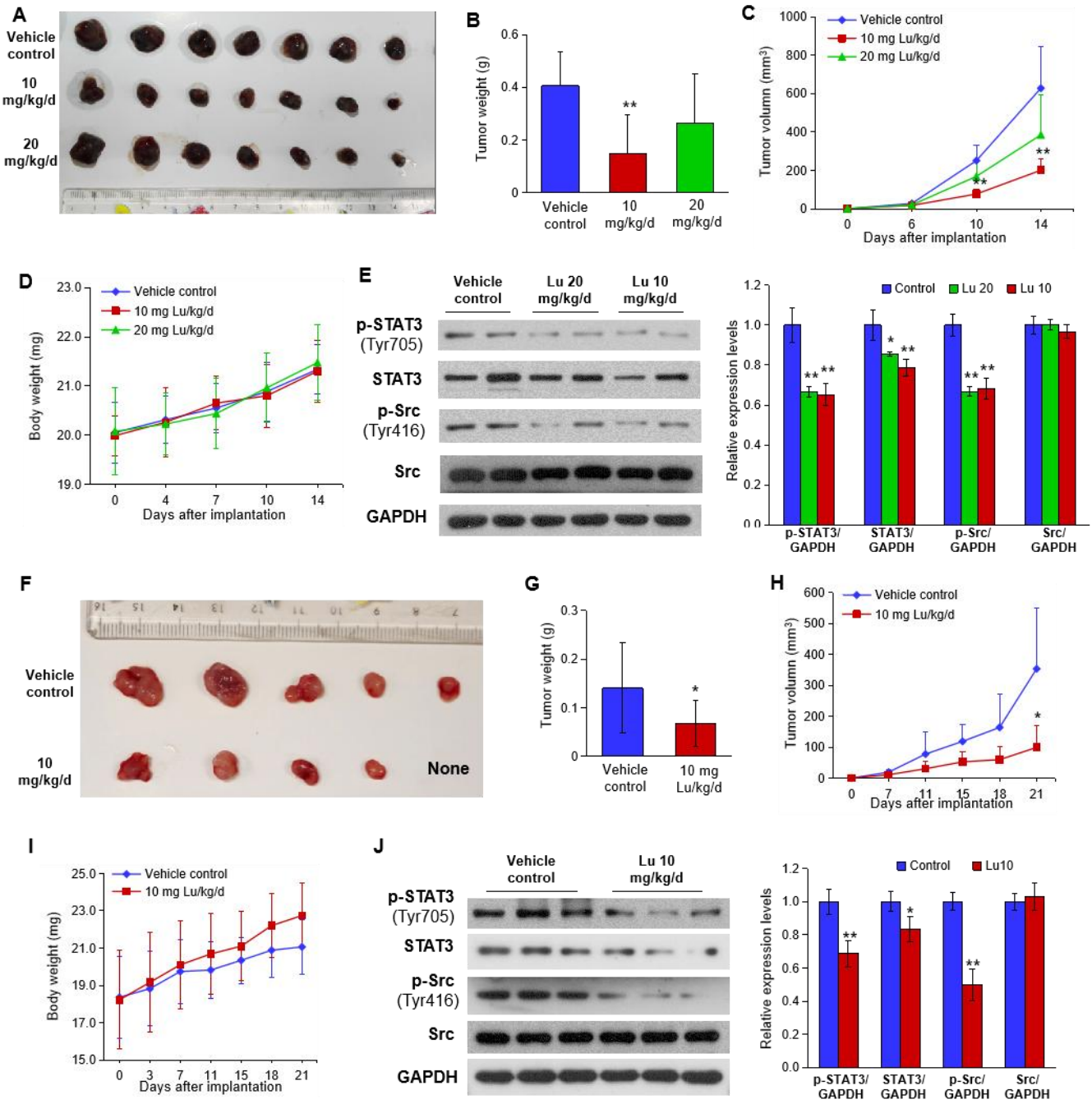

782

783 **Figure 7**

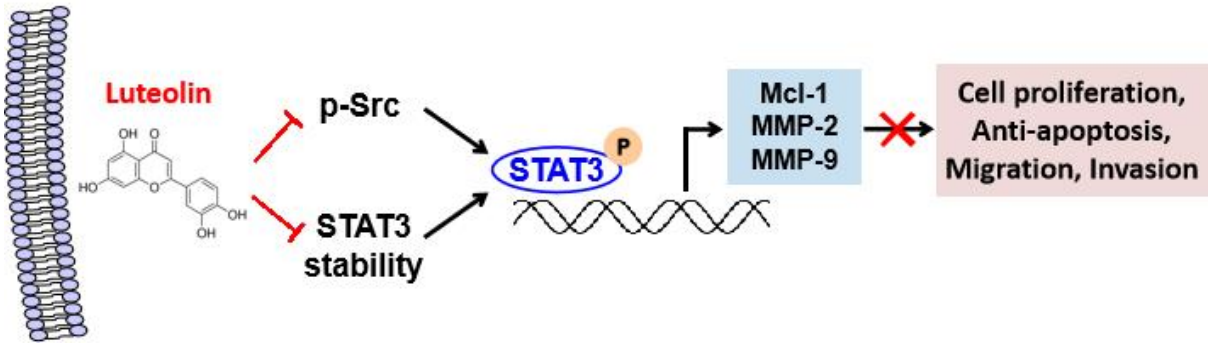

784